551.509.317 : 681.14

The computation of forecast charts by application of the Sawyer-Bushby two-parameter model

By F. H. BUSHBY and MAVIS K. HINDS
Meteorological Office, Dunstable

(Manuscript received 16 December 1953, in revised form 11 February 1954)

SUMMARY

Two series of 12-hr and 24-hr forecast 500 mb, 1,000 mb and 1,000-500 mb thickness charts have been computed electronically using the Sawyer-Bushby (1953) two-parameter baroclinic model of the atmosphere. The results are compared with the actual charts, and a good degree of correspondence is found between the actual and computed charts.

1. INTRODUCTION

Several authors have recently suggested that the large-scale atmospheric motions could be predicted by the application of numerical methods of mathematical analysis to equations which represents the motion in various simplified models of the atmosphere. Charney and his colleagues at The Institute for Advanced Study, Princeton, have investigated the barotropic model atmosphere and Charney, Fjörtoft and von Neumann (1950) have given the results of some 12-hr and 24-hr forecasts of the 500-mb contour surface based on this model. More recently Charney and Phillips (1953) give the results of some 12-hr and 24-hr forecasts based on the two-layer barotropic model. Alternatively, some of the baroclinic features of the atmosphere can be incorporated in a simple two-parametric baroclinic model by assuming that the variation of the horizontal and vertical components of velocity with height is the same along all verticals. Eady (1952), Eliassen (1952), Sawyer and Bushby (1953) and Thompson (1953) have derived sets of equations which describe the motions in particular versions of this model.

The model of the atmosphere used by Sawyer and Bushby consists of a baroclinic fluid in which the thermal wind is constant in direction in any vertical column but not necessarily parallel to the wind direction at any level, and the thermal wind speed is assumed proportional to the pressure difference through the layer concerned. The atmosphere is considered bounded by two pressure surfaces across which the movement of the air is assumed to be negligible, one pressure surface, $p = p_1$, corresponding to a level near the tropopause and one, $p = p_0$, corresponding to a level near the ground. The variation of the vertical motion with respect to pressure is assumed to be parabolic, and the geostrophic approximation is made after the horizontal divergence has been eliminated from the equations.

The present paper gives the result of 12-hr and 24-hr forecasts based on the Sawyer-Bushby model for two synoptic situations but the computations in each case were done well after the event. The computed charts, subsequently referred to as forecast charts, are compared with the actual charts and an attempt is made to estimate the effect of computational instability and arbitrarily chosen boundary conditions on the answers.

2. EQUATIONS

The state of the atmosphere in the Sawyer-Bushby model is specified by the two parameters h_m, the height of the central pressure level of the layer from $p = p_0$ to $p = p_1$ (at $p = p_m$) and h', the thickness of the layer from p_0 to p_m. The method is one in which

the instantaneous rates of change of h_m and h' are computed for time t using values of h_m and h' at that time and from these calculated rates of change the values of h_m and h' are obtained for a later time $t + \delta t$. The process is then repeated n times and forecast charts are produced for time $t + n\delta t$.

Eliminating Π_m (where $\Pi = dp/dt$, a measure of vertical motion, and the suffix m refers to the value at the level $p = p_m$) from the equations derived by Sawyer and Bushby, and neglecting the term representing the vertical advection of vorticity, the following equations can be derived for $\partial h_m/\partial t$ and $\partial h'/\partial t$:

$$\nabla^2 \partial h_m/\partial t + J(h_m, \beta^2 gl^{-1} \nabla^2 h_m + l) + \tfrac{1}{3} J(h', \beta^2 gl^{-1} \nabla^2 h') = 0 \quad . \quad (1)$$

$$\nabla^2 \partial h'/\partial t + \frac{4g(\nabla^2 h_m + l^2/\beta^2 g)\{\beta^2 gl^{-1} J(h_m, h') + \partial h'/\partial t\}}{RA\,\Gamma_p (p_0 - p_1)} + J(h_m, \beta^2 gl^{-1} \nabla^2 h') + J(h', \beta^2 gl^{-1} \nabla^2 h_m + l) = 0 \quad . \quad (2)$$

where

$$A \equiv \frac{p_0 + 3p_1}{2(p_0 - p_1)} - \frac{4p_0 p_1}{(p_0 - p_1)^2} \ln \frac{2p_0}{p_0 + p_1},$$

∇^2 and J are the two-dimensional Laplacian and Jacobian operators referred to rectangular Cartesian co-ordinates in the stereographic projection of the northern hemisphere on to a plane perpendicular to the earth's axis passing through the north pole; β is the magnification factor $\sec^2(\pi/4 - \theta/2)$, θ being the geographical latitude; g is the acceleration due to gravity; l is the Coriolis parameter; R is the universal gas constant and Γ_p a measure of the departure of the lapse rate from the adiabatic given by $\Gamma_p = \partial T/\partial p - \gamma/g\rho$, γ being the appropriate wet or dry adiabatic lapse rate, ρ the density and T the absolute temperature. Justification of the neglect of the term representing the vertical advection of vorticity is given by Bushby and Hinds (1954).

The following system of equations was used for the time-integration process :

$$H_{n+1} = h_{n-1} + 2(\partial H/\partial t)_n \, \delta t \quad . \quad . \quad . \quad . \quad (3)$$

$$h_{n+1} = h_n + \tfrac{1}{2}[(\partial H/\partial t)_n + (\partial H/\partial t)_{n+1}] \, \delta t \quad . \quad . \quad (4)$$

where H_n represents the first approximation and h_n the second approximation to either h_m or h' at time $t + n\delta t$, and $\partial H/\partial t$ is the value of $\partial h_m/\partial t$ or $\partial h'/\partial t$ obtained from Eqs. (1) or (2) when the first approximations to h_m and h' are used in those equations. For the first step in the integration, values of h_m and h' are known only at one instant of time and it is necessary to replace the centred difference Eq. (3) by the forward-difference formula

$$H_1 = h_0 + (\partial h/\partial t)_0 \, \delta t \quad . \quad . \quad . \quad . \quad . \quad (5)$$

It was decided to use Eqs. (3) and (4), instead of Eq. (3) alone, for the time-integration procedure in an attempt to reduce the effect of computational instability.

The computations were carried out partly on LEO, an electronic computing machine owned by Messrs. J. Lyons and Co. Ltd., and partly on a Ferranti machine at Manchester University. The finite-difference approximations to Eqs. (1) and (2) were solved for $\partial h_m/\partial t$ and $\partial h'/\partial t$ using the technique described by Bushby and Hinds (1954). A rectangular grid of 18 × 14 points was used. As two rings of boundary points are lost in computing the finite-difference approximations to the vorticity-advection terms, Eqs. (1) and (2) were solved for a grid of 16 × 12 points including boundary points.

As these computations were necessarily experimental rather than routine in nature, the results were printed after each step in the time-integration process. This increased

the length of time spent in completing one cycle of the calculation, but with recent additions of high-speed input and output equipment to LEO, it is now possible to complete one cycle of the computation in about nine minutes on either machine. As it takes about five minutes to get the programme and initial data into the machine, it would take approximately $(5 + 9n)$ min to complete a forecast for time $t + n\delta t$, given initial data at time t.

In the present work the values of p_0 and p_1 were taken to be 1,000 mb and 200 mb respectively. This would give $p_m = 600$ mb, a level for which charts are not normally available. h_m was therefore identified with the height of the 500-mb surface and h' with the thickness of the 1,000-500 mb layer.

After consideration of previous computational results a constant value, 38°F per 500 mb, was taken for Γ_p.

3. Space and time increments

In order that the solution of the finite-difference approximations to Eqs. (1) and (2) should approximate closely to the continuous solution, the space and time increments δs and δt must be small in comparison with the space and time scales of the large-scale atmospheric systems. However, the smaller δs, the more grid points are necessary to cover a given area, and the computation time is increased. After some experimenting it was decided to use a value of δs which approximates to 260 km in middle latitudes.

Apart from the aforementioned considerations, it is also necessary to ensure that the small-scale irregularities in the fields of h_m and h' do not amplify during the integration process. The computation is said to be unstable when such amplification takes place. Owing to the complex nature of the equations involved, it is extremely difficult to derive rigorously the conditions necessary for stability, but it is apparent that the ratio $\delta s/\delta t$ has to lie within certain limits.

From general considerations, it was decided to commence the computations with δt equal to two hours. It could be seen from inspection of the results that the integration based on the initial data of 15 GMT 27 January 1952 was unstable after the 18-hr stage. The distortions had increased in amplitude by the 24-hr stage but did not affect the region of the British Isles, for which a reasonable 24-hr forecast was computed. The computations were then repeated but δt was changed to one hour when the 12-hr stage was reached. This removed all trace of instability (see Figs. 1-3).

During the integration based on the initial data of 15 GMT 14 March 1949, instability became apparent after the 10-hr stage and considerable amplification and distortion over most of the chart had taken place by the 12-hr stage. The computation was stopped and restarted from the 8-hr stage, using δt equal to one hour. The calculations then remained stable over the whole of the chart for the remainder of the forecast period (Figs. 4-6).

Charney *et al.* (1950), when solving the barotropic equation, using a centred-difference formula for the time integration, derived the following approximate relationship

$$\frac{\delta s}{\delta t} \geqslant \sqrt{2}\,\beta\, v \qquad . \quad . \quad . \quad . \quad (6)$$

where v is the maximum particle speed in the forecast region, as giving a lower bound to the stability criterion. If the same relationship is applied to the present set of equations, then with δt = two hours, the computations would become unstable if v were greater than 60 kt in middle latitudes. It is thought that the present method of time integration is more stable than the simple centred-difference formula used by Charney *et al.* (1950), but the problem of computational instability is at present being further investigated in the Forecast Research Division at Dunstable.

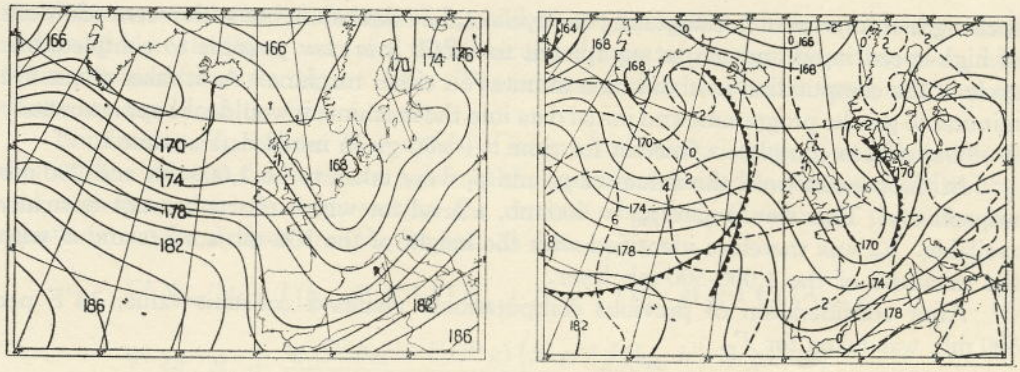

Figure 1. 15 GMT, 27 Jan. 1952. (a) Actual 500 mb chart; (b) Actual 1,000 mb and 1,000-500 mb thickness charts. ———— 1,000-500 mb thickness lines, - - - - 1,000 mb contours.

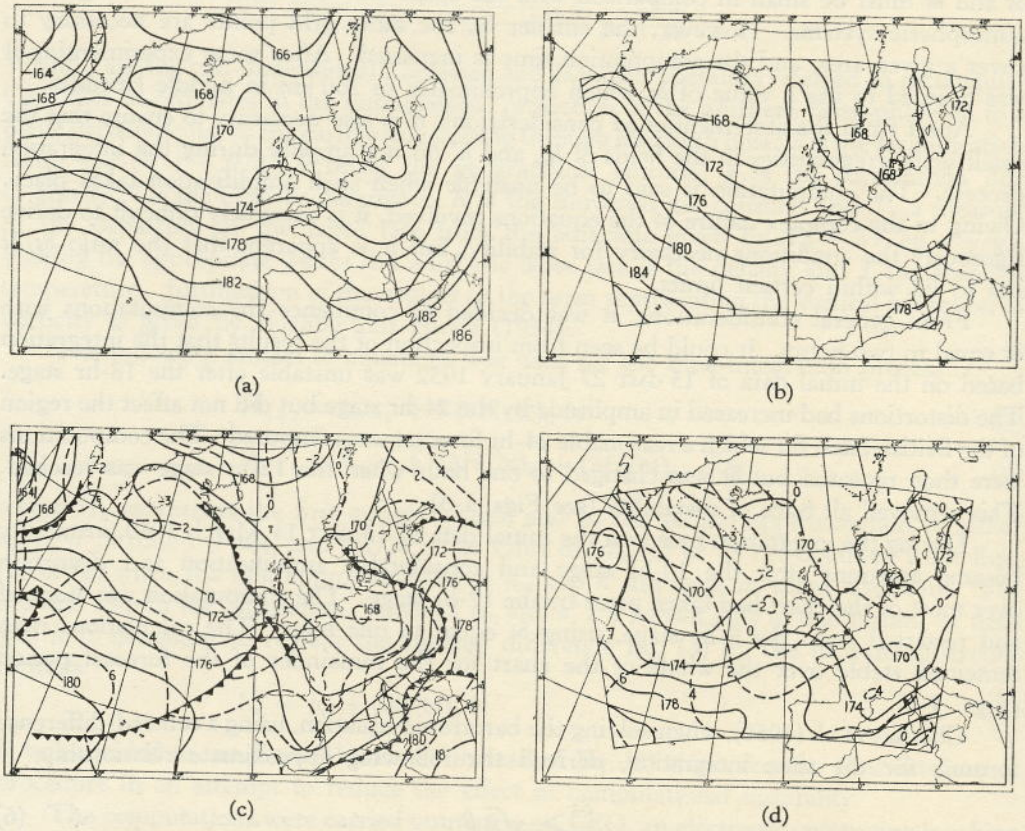

Figure 2. 03 GMT, 28 Jan. 1952. (a) Actual 500 mb chart; (b) Computed 500 mb chart; (c) Actual 1,000 mb and 1,000-500 mb thickness charts; (d) Computed 1,000 mb and 1,000-500 mb thickness charts. ((c) and (d) ———— 1,000-500 mb thickness lines, - - - - 1,000 mb contours)

4. Boundary conditions

A sufficient boundary condition for the solution of Eqs. (1)-(5) in a given region is that h_m, h', $\nabla^2 h_m$ and $\nabla^2 h'$ should be given along the boundary of that region. Thus when the finite-difference approximations to Eqs. (1)-(5) are being solved, it is necessary

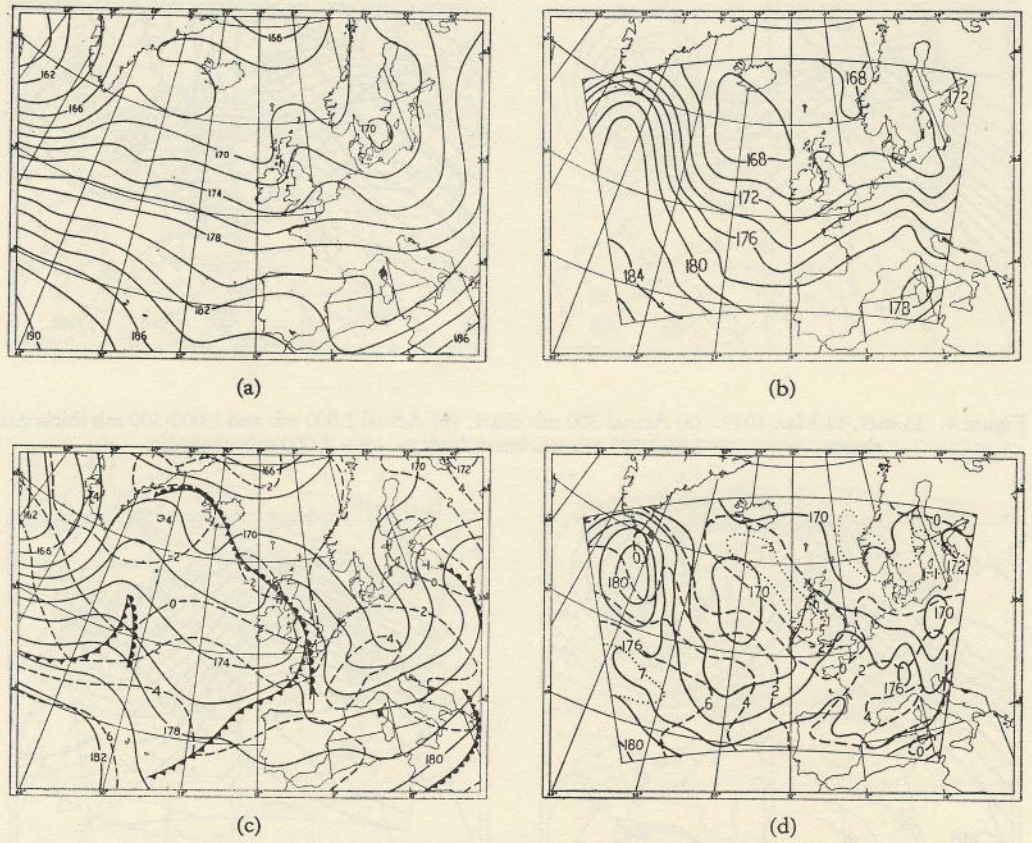

Figure 3. 15 GMT, 28 Jan. 1952. (a) Actual 500 mb chart; (b) Computed 500 mb chart; (c) Actual 1,000 mb and 1,000-500 mb thickness charts; (d) Computed 1,000 mb and 1,000-500 mb thickness charts. ((c) and (d) ——— 1,000-500 mb thickness lines, - - - - 1,000 mb contours)

to specify the values of h_m, h', $\nabla^2 h_m$ and $\nabla^2 h'$ at all grid points on the boundary (except corner points) or alternatively to specify the values of h_m and h' at all grid points on the boundary and at all grid points immediately exterior to the boundary. The second of these two alternatives was used in the present computations.

It was considered that the arbitrary boundary values would not affect significantly the centre of the forecast region by the end of the forecast period. The boundary values assigned to h_m and h' have to be chosen quite arbitrarily, because unless one considers the whole of the northern hemisphere in order to make use of the observed fact that h_m and h' show little variation near the equator, there are no conclusive reasons for pre-determining the values of h_m and h' along the boundary. The following boundary values were chosen as they are quite simple and tend to smooth the field of h_m and h' in a direction normal to the boundary in the vicinity of the boundary.

The initial data used in the computations were the values of h_m and h' at the points of the 18 × 14 grid. This enabled the Poisson and Helmholtz Equations (1) and (2) to be solved for $\partial h_m/\partial t$ and $\partial h'/\partial t$ at 16 × 12 points, including the boundary points at which values of $\partial h_m/\partial t$ and $\partial h'/\partial t$ were assumed zero. However in using Eqs. (3), (4) and (5) for the time integration, $\partial h_m/\partial t$ and $\partial h'/\partial t$ were taken as zero at the boundary points of the 18 × 14 grid; at the boundary points of the internal 16 × 12 grid, $\partial h_m/\partial t$ and $\partial h'/\partial t$ were now taken equal to half the value at the immediate interior point except that

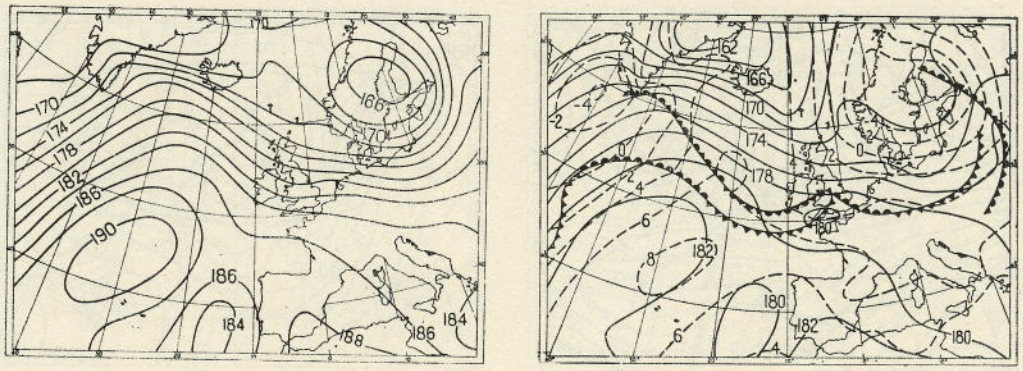

Figure 4. 15 GMT, 14 Mar. 1949. (a) Actual 500 mb chart; (b) Actual 1,000 mb and 1,000-500 mb thickness charts. ——— 1,000-500 mb thickness lines, - - - - 1,000 mb contours.

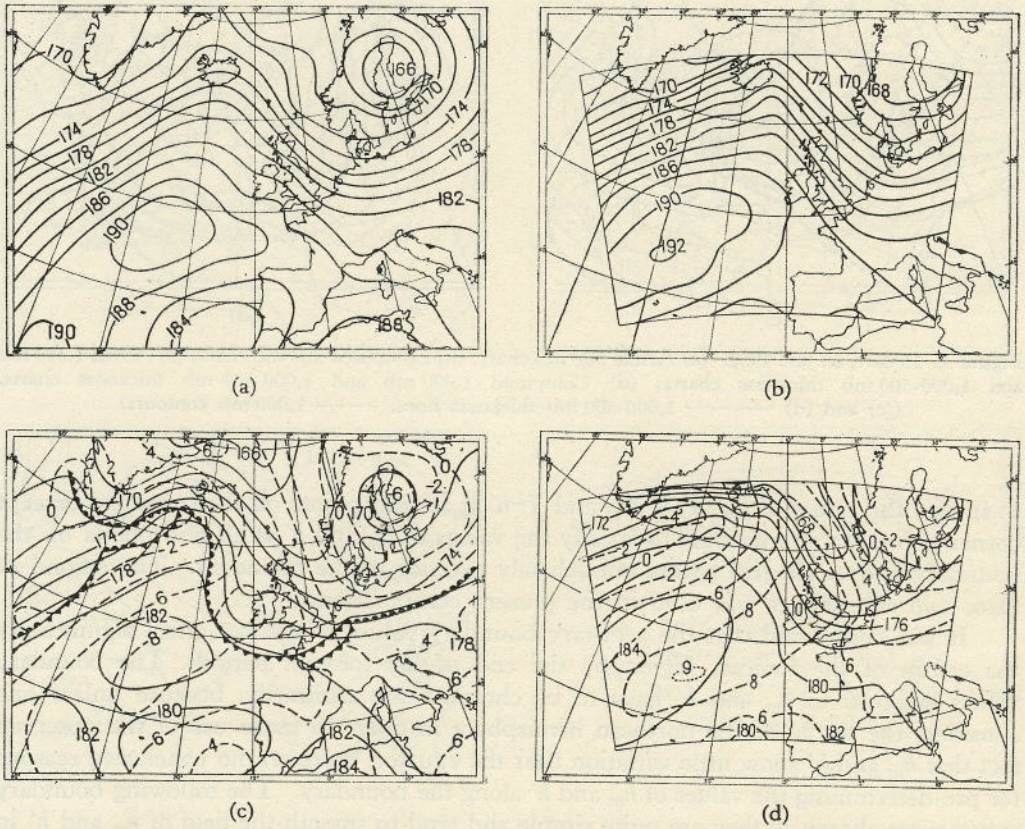

Figure 5. 03 GMT, 15 Mar. 1949. (a) Actual 500 mb chart; (b) Computed 500 mb chart; (c) Actual 1,000 mb and 1,000-500 mb thickness charts; (d) Computed 1,000 mb and 1,000-500 mb thickness charts. ((c) and (d) ——— 1,000-500 mb thickness lines, - - - - 1,000 mb contours)

at the four corner points a value of one-quarter of that at the nearest interior point was used. In the accompanying diagrams the computed results are shown for the area represented by the 16 × 12 internal points of the grid (this area does not appear rectangular as a conical orthomorphic background chart has been used).

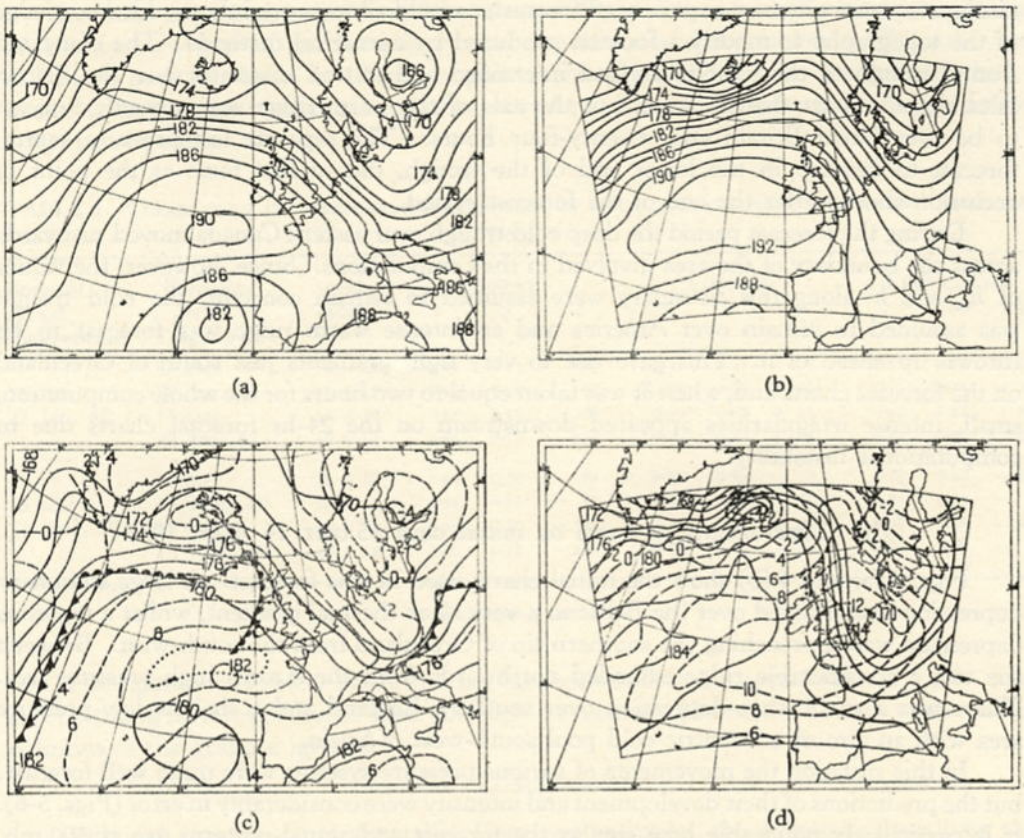

Figure 6. 15 GMT, 15 Mar. 1949. (a)Actual 500 mb chart; (b) Computed 500 mb chart; (c) Actual 1,000 mb and 1,000-500 mb thickness charts; (d) Computed 1,000 mb and 1,000-500 mb thickness charts. ((c) and (d) ——— 1,000-500 mb thickness lines, – – – – 1,000 mb contours)

5. Results

(a) *Time-integration based on initial data for* 15 GMT 27 *January* 1952

The initial charts on which this computation is based are shown in Figs. 1 (a) and 1 (b). The situation was one in which there was a broad westerly flow across the North Atlantic at 500 mb, with large-amplitude troughs over eastern Canada and western Europe and an intermediate shallower trough south-east of Greenland. Surface and thickness patterns were also largely westerly over the Atlantic, but over western Europe the surface-pressure gradient was flat and mainly cyclonic, there being a tongue of deep cold air down the North Sea into northern France.

During the ensuing twenty-four hours the cold trough over the North Sea moved slowly eastwards to Scandinavia and eastern Germany, the associated surface trough also moving away eastwards. The movements of this feature were well forecast, the axis of the 500 mb trough being in almost the correct position on each of the forecast charts (Figs. 2 and 3). The surface low-pressure area, however, was not forecast to move far enough eastwards. Behind the base of the cold trough, the ridge originally over the Bay of Biscay was forecast to intensify considerably and move eastwards to reach a position over northern Italy after twenty-four hours. The ridge moved as forecast for the first twelve hours but thereafter, possibly owing to the close proximity of the Alps, moved more north-eastwards than forecast. This is a particularly marked example of a

circumstance in which an experienced forecaster would almost certainly use his knowledge of the topography to modify a forecast produced by numerical methods. The elongated frontal trough to the west of Ireland intensified and moved eastward over the British Isles slightly faster than forecast, but the axis of the warm ridge was correctly forecast to be over Great Britain after twenty-four hours. The separate low-pressure centre, forecast to develop in the lower end of the trough, did in fact form at the point of occlusion shortly after the end of the forecast period.

During the forecast period the deep cold trough over eastern Canada moved eastwards across the boundary of the area involved in the computations. Since, however, the values of h_m and h' along this boundary were assumed to remain constant, the cold trough was assumed to remain over America and an intense warm ridge was forecast to be thrown up ahead of it. This gave rise to very tight gradients just south of Greenland on the forecast charts and, when δt was taken equal to two hours for the whole computation, small, intense irregularities appeared downstream on the 24-hr forecast charts due to computational instability.

(b) *Time-integration based on initial data* 15 GMT 14 *Mar.* 1949

Figs. 4 (a) and 4 (b) show the initial charts used in this forecast. A large stationary depression was situated over the Baltic in a very slack thermal gradient, whilst a vigorous depression was approaching the southern tip of Greenland from the south-west. Between the two a considerable ridge extended northwards from the Azores high-pressure area. There was a small wave-depression over southern England and a shallow low-pressure area with an almost concentric cold pool south-west of Spain.

In this situation the movements of various pressure systems were quite well forecast, but the predictions of their development and intensity were considerably in error (Figs. 5-6). It is particularly noticeable how similar the forecast and actual patterns are at 500 mb, the main errors in the forecast being the intensification of the ridge north of the Azores and the small trough west of Iceland.

During the forecast period the wave depression moved rapidly away into Russia and was followed by a mobile ridge which spread down into southern England and France and was absorbed into the considerably enlarged Azores anticyclone. On the forecast charts the oscillation in the thickness pattern was predicted to intensify too much, giving a very strong westerly thermal gradient over Iceland and northerly thermal gradient over the British Isles. This oscillation gave a very marked anticyclonic development area over the British Isles and in consequence the mobile ridge was forecast to develop into an extremely intense high-pressure area with the Azores anticyclone as a ridge extension.

The depression approaching the tip of Greenland at the beginning of the period was forecast to split into two parts, a shallow low-pressure area in the Davis Strait and a more intense depression moving north-eastward to Iceland. This movement actually occurred but the depression over Iceland was less deep that it was forecast to be.

(c) *Correlation and regression coefficients*

Correlation coefficients have been calculated comparing computed changes with actual changes over 12-hr and 24-hr periods starting from the initial data. Regression coefficients were calculated for the best fitting straight lines giving the actual change (Y feet) in terms of the computed change (X feet) in the form

$$Y = bX + c \quad . \quad . \quad . \quad . \quad (7)$$

In order to gain an indication of the adverse effects of the wrong boundary conditions on the western part of the forecast charts, correlation and regression coefficients were calculated both for the 16 × 12 grid of points over which the contour heights and thicknesses were forecast to change, and also over the same area without the six westernmost columns of points.

TABLE 1. CORRELATION AND REGRESSION COEFFICIENTS OF ACTUAL AND COMPUTED HEIGHT AND THICKNESS CHANGES

Forecast period commencing	Forecast period ending	grid size	500mb			1,000 mb			1,000-500 mb		
			r	b	c	r	b	c	r	b	c
	03 GMT	16 × 12	0·41	0·43	36	0·35	0·47	− 3	0·55	0·46	24
15 GMT	28 Jan. 52	10 × 12	0·82	0·98	92	0·71	0·67	60	0·77	0·78	− 4
27 Jan. 52	15 GMT	16 × 12	0·18	0·15	29	0·49	0·67	− 15	0·42	0·27	30
	28 Jan. 52	10 × 12	0·84	0·72	139	0·79	0·78	101	0·76	0·56	28
	03 GMT	16 × 12	0·66	0·58	− 30	0·81	0·59	7	0·78	0·82	− 51
15 GMT	15 Mar. 49	10 × 12	0·84	0·83	− 47	0·90	0·70	− 22	0·85	0·80	− 8
14 Mar. 49	15 GMT	16 × 12	0·69	0·59	− 97	0·76	0·47	− 33	0·81	0·64	− 44
	15 Mar. 49	10 × 12	0·76	0·71	− 133	0·83	0·52	− 68	0·94	0·68	− 1

r = correlation coefficient

The figures in Table 1 confirm what has been said in Sections 5 (a) and 5 (b). The most striking features of Table 1 are the high correlations obtained if the six westernmost columns of the grid are ignored.

6. CONCLUSIONS

Although one must not generalize from two examples, the equations describing the motion in the Sawyer-Bushby two-parameter baroclinic model atmosphere give, in the two situations so far considered, a fair representation of the motion in the real atmosphere for a 24-hr period, in the regions not affected by the arbitrary choice of boundary conditions. In order to avoid computational instability it appears necessary to use a time step of one hour, but even so it is possible to compute a 24-hr forecast in under four hours. If the present rate of development of electronic computing machinery is maintained, it should be possible to make a significant reduction in this time.

ACKNOWLEDGMENTS

The authors wish to thank the Director of the Meteorological Office for permission to publish this paper and to acknowledge the assistance given by Mr. J. S. Sawyer, Miss D. L. Pritchard and Miss A. D. Robson. We also wish to thank Mr. R. A. Brooker of Manchester University and the staff of Messrs. J. Lyons and Co., Ltd. for their help during the use of the electronic computing machines.

REFERENCES

Bushby, F. H. and Hinds, M. K. 1954 *Quart. J. R. Met. Soc.*, **80**, p. 16.
Charney, J. G., Fjörtoft, R. and von Neumann, J. 1950 *Tellus*, **2**, p. 237.
Charney, J. G. and Phillips, N. A. 1953 *J. Met.*, **10**, p. 71.
Eady, E. T. 1952 *Tellus*, **4**, p. 157.
Eliassen, A. 1952 *Ibid*, **4**, p. 145.
Sawyer, J. S. and Bushby, F. H. 1953 *J. Met.*, **10**, p. 54.
Thompson, P. D. 1953 *Quart. J. R. Met. Soc.*, **79**, p. 51.